Langmuir

Article

pubs.acs.org/Langmuir

Overlimiting Current and Shock Electrodialysis in Porous Media

Daosheng Deng,[†] E. Victoria Dydek,[†,§] Ji-Hyung Han,[†] Sven Schlumpberger,[†] Ali Mani,[†,∥] Boris Zaltzman,[†,⊥] and Martin Z. Bazant*[,†,‡]

[†]Department of Chemical Engineering and [‡]Department of Mathematics, Massachusetts Institute of Technology, Cambridge, Massachusetts 02139 United States

Supporting Information

ABSTRACT: Most electrochemical processes, such as electrodialysis, are limited by diffusion, but in porous media, surface conduction and electroosmotic flow also contribute to ionic flux. In this article, we report experimental evidence for surface-driven overlimiting current (faster than diffusion) and deionization shocks (propagating salt removal) in a porous medium. The apparatus consists of a silica glass frit (1 mm thick with a 500 nm mean pore size) in an aqueous electrolyte ($CuSO_4$ or $AgNO_3$) passing ionic current from a reservoir to a cation-selective membrane (Nafion). The current−voltage relation of the whole system is consistent with a proposed theory based on the electroosmotic flow mechanism over a broad range of reservoir salt concentrations (0.1 mM to 1.0 M) after accounting for (Cu) electrode polarization and pH-regulated silica charge. Above the limiting current, deionized water (≈10 μM) can be continuously extracted from the frit, which implies the existence of a stable shock propagating against the flow, bordering a depleted region that extends more than 0.5 mm across the outlet. The results suggest the feasibility of shock electrodialysis as a new approach to water desalination and other electrochemical separations.

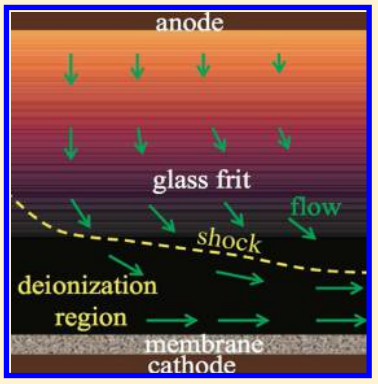

INTRODUCTION

Electrochemistry is playing an increasingly important role in sustainable world development. Besides energy conversion and storage, electrochemical systems also provide unique capabilities for desalination and other separations. The availability of fresh water may soon exceed that of energy as a global concern, which will require advances in water purification technologies.[1−4] Water treatment is also a key challenge for energy-related industrial processes, such as hydraulic fracturing ("fracking") for shale gas extraction.[5] The most difficult step is the removal of dissolved salts, especially multivalent ions.[6−8] Reverse osmosis (RO) driven by mechanical pressure is widely used for large-scale seawater desalination but is costly and energy-intensive. Electrochemical methods, such as electrodialysis[9,10] (ED) and capacitive deionization[11] (CD), can be attractive for brackish or wastewater treatment and for compact, portable systems.

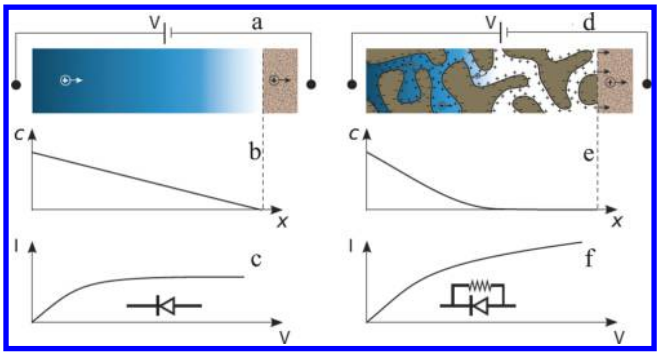

Figure 1. Steady ion concentration polarization from a reservoir to an ideal cation-selective membrane through a bulk electrolyte (a), where the salt vanishes at the membranes (b) at the diffusion-limited current (c) analogous to the diode or through a negatively charged porous medium with thin double layers (d), where surface transport enables a broad depleted region (e) and a nearly constant overlimiting conductance (f), acting as a shunt resistance.

The rate-limiting step in electrochemical separations, including ED[10] and CD,[11] is typically diffusion. The classical diffusion-limited current arises when cations are completely removed at a membrane or electrode surface as anions are rejected to maintain neutrality (Figure 1a). For a dilute z/z electrolyte, ambipolar diffusion leads to a linear concentration profile at steady state (Figure 1b), and the current−voltage relationship,[9,12]

$$I = I_{\lim}\left[1 - \exp\left(-\frac{zeV}{k_B T}\right)\right] \quad (1)$$

is equivalent to that of an ideal diode (Figure 1c), where

$$I_{\lim} = \frac{2zeDc_0}{L}A \quad (2)$$

is the diffusion-limited current, A is the area of the current collector, I is the measured current, V is the voltage across the electrolyte, k_B is Boltzmann's constant, T is the temperature, e is

Received: January 31, 2013
Published: December 9, 2013

the electron charge, D is the cation diffusion coefficient, c_0 is the reservoir ion concentration, and L is the diffusion length from the reservoir to the selective surface. Above the thermal voltage, $V \gg k_BT/e$ (= 26 mV at room temperature), the current saturates, $I \to I_{lim}$, like a diode under reverse bias.

In practice, an overlimiting current (OLC), which exceeds I_{lim}, is often observed, and its possible origins have long been debated.[10] For bulk transport, the consensus is that OLC can arise from chemical effects, which create more ions[10,13] or reduce membrane selectivity,[14] or from convection by electroosmotic instability near the membrane.[15−18] More intriguingly, it has recently been predicted that surface transport can also sustain OLC in a microchannel by electroosmotic flow[19] (EOF) or surface conduction[12] (SC) along the side walls, depending on the aspect ratio and surface charge. The new theory[12] may explain different ion concentration polarization (ICP) phenomena observed at micro/nanochannel junctions.[20,21]

A surprising feature of microfluidic experiments in the regime of overlimiting current is the tendency for the depleted region to form a very sharp boundary with the bulk electrolyte,[20,22,23] which can be understood as a shock wave in the salt concentration, propagating against the flow.[24−26] It has recently been predicted that stable "deionization shocks" can also propagate in porous media at constant current,[27−29] and the theory predicts steady OLC in a finite system at constant voltage (Figure 1d−f).[12,28,29]

In this article, we investigate OLC experimentally in materials with a submicrometer mean pore size. The results are consistent with theoretical predictions and reveal some basic principles of nonlinear electrokinetics in porous media. Classical electrokinetic phenomena, such as the streaming potential and electroosmotic flow, are defined by the linear response of flow or current to a small applied voltage or pressure,[9] but relatively little is known about the nonlinear response of a porous medium to a large voltage ($V \gg k_BT/e$ = 26 mV at room temperature). In contrast to recent work on induced-charge electrokinetics in polarizable media,[30] we focus on surfaces of (nearly) fixed charge and report the first experimental evidence that surface transport can sustain OLC and deionization shocks over macroscopic distances in a porous medium.

THEORY

Overlimiting Conductance. The classical theory of ICP assumes a homogeneous bulk electrolyte,[9] but there is a growing realization that new nonlinear electrokinetic phenomena arise when the electrolyte is weakly confined by charged surfaces aligned with the applied current.[12,19,24−29,31−33] Under strong confinement with overlapping double layers, a nanochannel or pore acts as a counterion-selective membrane because the pore is effectively "all surface".[34] Under weak confinement with thin double layers, it is well known that surface conduction plays only a small role in linear electrokinetic phenomena because the total excess surface conductivity is much smaller than the total bulk conductivity (small Dukhin number).[35] ICP alters this picture, and surprisingly, surface-driven transport can dominate at high voltage, even with initially thin double layers.

A simple theory of OLC in a microchannel was recently proposed by our group.[12] In thin or highly charged channels, the dominant mechanism is SC, and in thick or weakly charged channels, it is EOF, as long as the viscosity is also low enough

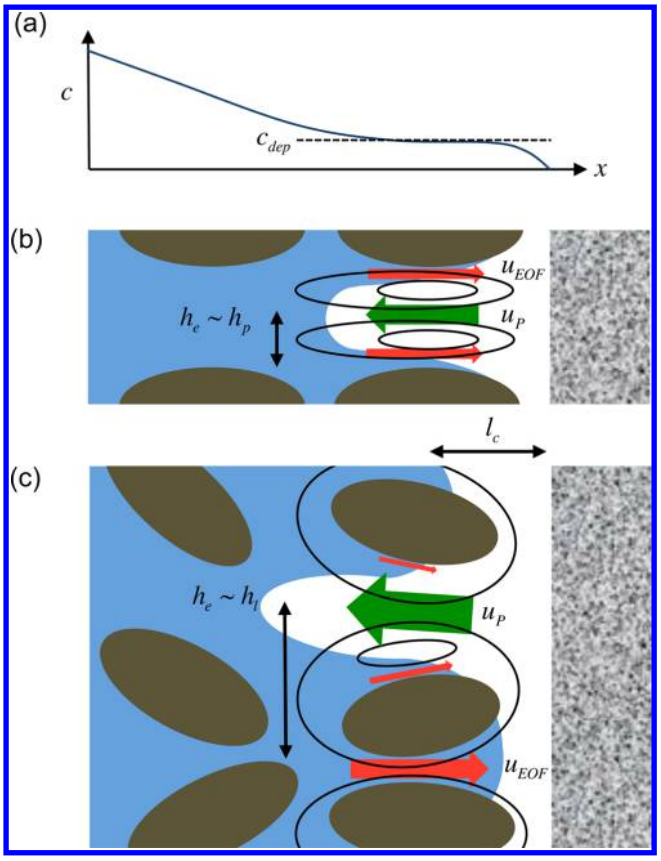

Figure 2. Electroosmotic flow (EOF) mechanism for overlimiting current through a porous medium (brown) to an impermeable counterion-selective membrane (right). Strong EOF (red arrows) in the depleted region and pressure-driven back flow (green arrows) produce salty (blue) and depleted (white) fingers in eddies of transverse size, h_e, centered at l_c. (a) Mean salt concentration profile. (b) In a regular microstructure, eddies are confined to parallel pores of size $h_e \approx h_p$. (c) In an irregular microstructure, eddies form around connected loops of width $h_e \approx h_l$.

for sufficiently fast flow. In water with typical surface charges, the predicted transition from SC to EOF occurs at the scale of several micrometers for dilute electrolytes (mM) or tens of nanometers for concentrated electrolytes (M). For both mechanisms, the current−voltage relationship is approximately linear just above the limiting current

$$I = I_{lim}\left[1 - \exp\left(-\frac{zeV}{k_BT}\right)\right] + \sigma_{OLC}V \tag{3}$$

as if the surfaces provide a constant shunt resistance to bypass the diodelike response of ICP (Figure 1f). The scalings of σ_{OLC} with salt concentration and surface charge allow the mechanism to be distinguished (below), but first we must generalize the theory to porous media.

Mechanism 1: Surface Conduction. Even during strong ICP the homogenized effect of SC in porous media without flow can be rigorously described by a volume-averaged electroneutrality condition.[27−29] For 1D transport over a distance L from a reservoir to an ideal cation-selective surface in a dilute binary electrolyte, the exact solution yields eq 3 with

$$\sigma_{OLC}^{SC} \approx \frac{2zeAD_m q_s}{k_BTLh_p} \tag{4}$$

dx.doi.org/10.1021/la4040547 | Langmuir 2013, 29, 16167−16177

where D_m is the macroscopic diffusivity, $-q_s$ is the (negative) pore surface charge per area, and $h_p = a_p^{-1}$ is the mean pore size equal to the inverse of a_p, the internal area density (area/volume)).[12,29] In the absence of flow, we have $D_m = \varepsilon_p D_0/\tau_p$, where D_0 is the molecular diffusivity in free solution, ε_p is the porosity, and τ_p is the tortuosity. Electroosmotic convection in the double layers contributes a small ~10% correction to the surface conductivity in a dead-end channel,[12] which can be neglected in thin pores. The primary effect of EOF is hydrodynamic dispersion, which increases the effective D and provides a second mechanism for OLC.

Mechanism 2: Electroosmotic Flow. As the pore width is increased, convection by EOF eventually dominates SC. The possibility of OLC sustained by EOF was first proposed by Yaroshchuk et al. on the basis of a Taylor-Aris dispersion model, but the assumption of slow convection compared to transverse diffusion is typically violated.[19] Dydek et al. then showed that EOF can support OLC by fast electroosmotic convection in the depleted region (Figure 2a), leading to nonuniform salt profiles with a thin boundary layer[12] (Figure 2b). Rubinstein and Zaltzman analyzed this new mode of dispersion in the simpler case of a neutral solute with constant slip velocity on the side walls and described "wall fingers" transitioning to spiral structures with increasing Péclet number.[33]

As a first approximation for EOF OLC in a porous medium, we adapt the microchannel scaling analysis of Dydek et al.[12] Electroosmotic flow scales as $u \sim \varepsilon\zeta E/\eta$, where the zeta potential, $\zeta \sim q_s\lambda_D/\varepsilon$, is related to the surface charge density q_s using the thin diffuse-layer capacitance ($C = \varepsilon/\lambda_D$). The mean tangential electric field, E, is related to the local mean current density, j, via $E \sim j/\sigma_b$, where $\lambda_D(c)$ is the Debye length and $\sigma_b(c)$ is the bulk conductivity, each depending on the local bulk salt concentration c. Combining these equations, we obtain the EOF velocity scaling, $u \sim q_s\lambda_D j/\sigma_b\eta$.

The porous medium is pressed against an impermeable, ideally selective membrane for counterions (opposite to the pore charge). To ensure zero mean flow, a pressure-driven backflow balances EOF and leads to hydrodynamic dispersion.[19] For a regular microstructure (Figure 2b), the sum of these flows is a vortex pair of width $h_e \sim h_p$ that produces parallel wall fingers.[12,33] For an irregular microstructure (Figure 2c), variations in hydraulic resistance lead to nonuniform backflow that can exceed the electroosmotic flow in the larger pores. In that case, the mean eddy size is set by connected loops between pores of high and low hydraulic resistance, $h_e \sim h_l$. As the current increases, the eddy fingers extend across larger distances, and the flow may even become chaotic, as with electroosmotic instability in free solution.[36] Nevertheless, the following simple theory manages to predict the scalings in our experiments.

Consider fast electroosmotic convection in the depleted region leading to eddy fingers of transverse thickness, h_e (set by the mean size of either pores or loops), and axial length l_c, set by the mean distance from the membrane to the eddy centers, as shown in Figure 2. As in boundary-layer analysis of forced convection in a pipe,[37] the convection–diffusion equation, $\vec{u}\cdot\nabla c = D_m\nabla^2 c$, then yields the scaling, $u/l_c \sim D_m/h_e^2$. As the eddy size increases at larger overlimiting currents, the effective diffusivity D incorporates porosity and tortuosity factors as well as corrections due to microscopic hydrodynamic dispersion (such as the Taylor dispersion) on length scales smaller than the eddy size. Combining the convection–diffusion scaling with the electroosmotic flow scalings above, we find $l_c \sim uh_e^2/D_m \sim q_s\lambda_D j h_e^2/\sigma_b\eta D_m$.

Assuming the same current–voltage relation as for a single microchannel (eq 8 in Dydek et al.[12]), the overlimiting conductance, $\sigma_{OLC} \sim 2(ze)^2 c_d D_m A/k_B TL$, is set by the mean salt concentration c_d in the depleted region (Figure 2a). Although this region contains fingers of nonuniform salt concentration, we use the mean value c_d to define the local bulk conductivity, $\sigma_b = \varepsilon D/\lambda_D^2$ and $\lambda_D^2 = \varepsilon k_B T/2(ze)^2 c$, respectively, as a first approximation. All that remains then is to determine c_d. Numerical simulations in a straight microchannel exhibit the scaling $c_d/c_0 \approx l_c/L$ close to the limiting current.[12] If the same relation also holds in a porous medium for $j \sim j_{lim} \sim 2zec_0 D_m/L$, then we can eliminate l_c and arrive at a scaling law for the overlimiting conductance,

$$\sigma_{OLC}^{EOF} \sim \frac{(2c_0 h_e)^{4/5} q_s^{2/5} (ze)^{6/5} \varepsilon^{1/5} D_m^{3/5} A}{(\eta k_B T)^{2/5} L^{9/5}} \quad (5)$$

where there is an unknown numerical prefactor that is independent of all the parameters. The best way to determine the prefactor, once the scalings are validated, is by experiment (below).

EXPERIMENT

Apparatus. The apparatus is designed to test the theoretical current–voltage relation (eq 3) for a charged porous medium and extract the overlimiting conductance. By choosing a copper electrolytic cell[38–40] with known Faradaic reaction resistance $R_F(c_0)$ and a porous silica glass frit with known surface charge q_s(pH) in water,[34,41,42] the

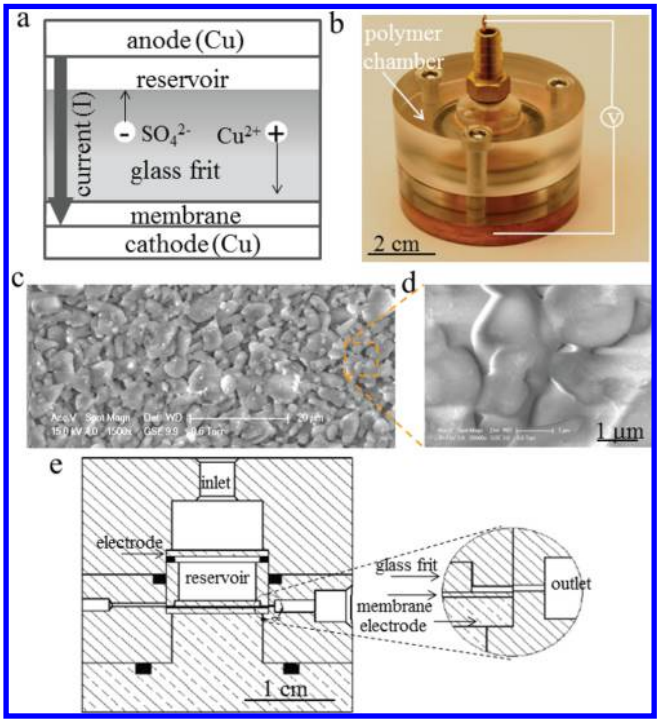

Figure 3. Prototype "button cell" for shock electrodialysis. (a) Sketch of the frit/membrane/electrode sandwich structure (not to scale), (b) photograph of prototype, (c) scanning electron microscopy (SEM) image of the glass frit showing the distribution of pores, and (d) enlarged micrographs consistent with the mean pore size of around 500 nm. (e) Cross-section drawing to scale. (Right) Enlargement showing the radial outlet for fresh water extraction.

dx.doi.org/10.1021/la4040547 | Langmuir 2013, 29, 16167–16177

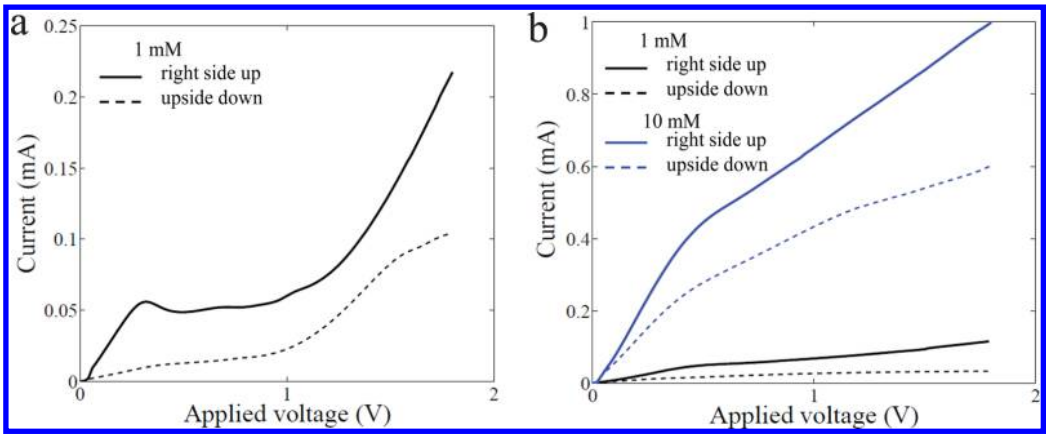

Figure 4. Effects of reservoir convection. (a) When the glass frit is removed, overlimiting current rises nonlinearly because of electroosmotic instability, and if the cell is upside down (cathode at the top), then the stable density gradient of copper sulfate depletion reduces the current. (b) When the glass frit is inserted, a linear overlimiting current (eq 3) is observed when the cell is right side up (cathode at the bottom) because of reservoir mixing by natural convection, but the transition to OLC is masked and the resistance is increased when the cell is upside down.

current–voltage relation of the frit can be isolated. The dependence of σ_{OLC} on c_0, which also involves q_s from measurements of pH(c_0), can be compared to theoretical formulas for the EOF and SC mechanisms, eqs 4 and 5, respectively, having clearly distinct scalings:

$$\sigma_{OLC} \sim \begin{cases} q_s & \text{SC} \\ {q_s}^{2/5} {c_0}^{4/5} & \text{EOF} \end{cases} \quad (6)$$

The dominant mechanism should have a larger predicted conductance.

The predicted salt depletion is directly tested by extracting deionized water from the glass frit by pressure-driven flow near the membrane interface. The flow rate is precisely controlled with a syringe pump (Harvard apparatus pump 33). The pH of the solution is measured by a pH meter (Thermo Scientific, Orion pH meter), and the conductivity is obtained by electrochemical impedance spectroscopy (Gamry Instrument reference 3000).

The key component of the apparatus is a cylindrical silica glass frit (L = 1 mm thick, R = 5 mm radius) pressed with screws against a Nafion membrane, in direct contact with a copper disk cathode (Figure 3). The frit is separated from a copper disk anode by an electrolyte reservoir (L_0 = 3 mm thick). The electrolyte is aqueous copper sulfate ($CuSO_4$), so the well-studied copper deposition/dissolution reaction[38−40,43]

$$Cu^{2+} + 2e^- \leftrightarrow Cu \quad (7)$$

is favored at both electrodes. Concentrated 1 M aqueous $CuSO_4$ solution is prepared by dissolving copper sulfate in the distilled water, and more dilute solutions are obtained by adding distilled water. The chamber is infused with the solution, and the glass frit and membrane are immersed in the solution for several hours prior to measurements. The frit (from Adams & Chittenden Scientific Glass) has a random microstructure of submicrometer pores, mostly 500−700 nm wide (Figure 3c,d) with a BET internal area of a_m = 1.75 m^2/g and a mass density of ρ_m = 1.02 g/cm^3. The pore area density, $a_p = a_m\rho_m = h_p^{-1}$, implies a mean pore size of h_p = 557 nm. As discussed below, the bare surface charge of the pores is regulated by pH, and some experiments are also done with two different chemical modifications to control the surface charge.

The Nafion membrane serves as the cation-selective surface in Figure 1, triggering salt depletion in the glass frit. In principle, the copper cathode could play this role by itself, but inserting the membrane better mimics theoretical models[12] and possible applications to water treatment below. The membrane also reduces the activation overpotential at the cathode (by maintaining a high cation concentration) and suppresses dendritic growth in the glass frit (as a result of pressurized contact with a space-filling material). Indeed, no dendrites are observed at the cathode, and the current is stable over the range of applied voltages. Nafion may also help to suppress hydrogen gas evolution at the copper cathode relative to electrodeposition because Cu^{2+} competes with H^+ in carrying the current while water reduction product OH^- is blocked.

Electrochemical Measurements. The current–voltage curves are measured using linear-sweep voltammetry with an electrochemical analyzer (Uniscan Instruments PG581). An optimal scan rate of 2 mV/s is chosen to attain a quasi-steady response while avoiding ICP in the reservoir, which develops over several hours at constant voltage. The typical time required to reach OLC at roughly 0.5 V is around 5 min, which is somewhat smaller than the diffusion time across the frit, $L^2/D \approx 20$ min. Along with convection in the reservoir (see below), this minimizes reservoir salt depletion but leaves some transient diffusion effects in the current versus time signals, namely, an initial bump or overshoot at the limiting current followed by weak oscillations around the approximately linear mean profile. Transient effects are also investigated by chronoamperometry in the Supporting Information.

A number of preliminary experiments are performed to validate the interpretation of the data below. We first confirm (Figure 4a) that eq 3 holds with the glass frit in place but changes to reflect the well-known nonlinear increase in OLC above a critical voltage due to electroosmotic instability[17] when the frit is removed. Next we consider natural convection due to buoyancy forces associated with copper sulfate depletion, which have been previously observed in copper electrodeposition experiments.[40,44] Copper sulfate is heavier than water, so the depleted fluid produced at the cathode tends to rise while the enriched fluid at the anode sinks. By repeating various experiments upside down, the effect of gravity becomes clear (Figure 4).

In our apparatus, buoyancy plays a crucial role by mixing the reservoir without significantly affecting transport within the glass frit. Natural convection is controlled by the Rayleigh number, $Ra = (\Delta\rho/\rho)gL^3/\nu D$, where $\Delta\rho/\rho$ is the relative fluid density variation, g is the gravitational acceleration, ν is the kinematic viscosity, D is the salt diffusivity, and L is the characteristic length scale. On the reservoir scale, L = 1 mm, natural convection is strong because $Ra = 10^7\Delta\rho/\rho$. When the system is right side up with the cathode producing lighter fluid at the bottom, the Rayleigh–Taylor instability vigorously mixes the reservoir because the Rayleigh number is much larger than the critical value $Ra \approx 10^3$. When upside down, lighter fluid is produced at the top of the cell, and the stable density gradient promotes slow diffusion into the reservoir, requiring many hours (L^2/D) to reach steady state and blurring the transition to overlimiting current (Figure 4b). The experimental setup thus exploits gravity to isolate the quasi-steady current–voltage relation of the glass frit from spurious effects of transient diffusion in the reservoir.

dx.doi.org/10.1021/la4040547 | Langmuir 2013, 29, 16167−16177

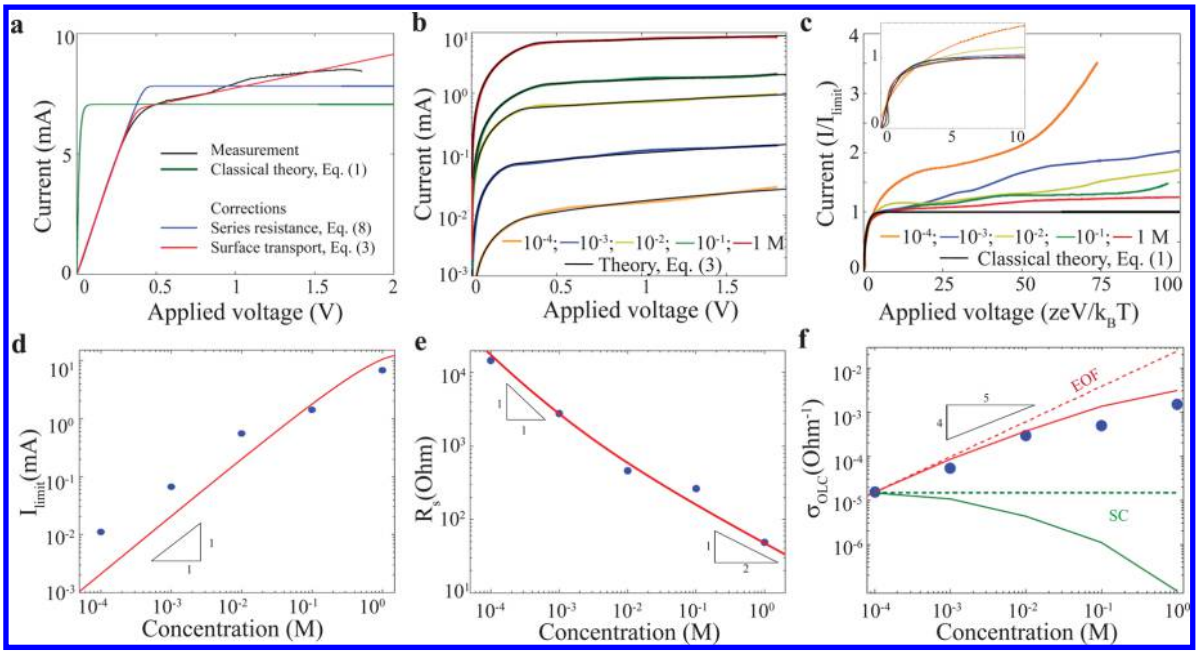

Figure 5. Observation of overlimiting current in aqueous $CuSO_4$. (a) For 1.0 M concentration, the current–voltage curve is compared to the classical diffusion-limited model (eq 1), the extension for OLC by surface transport (eq 3), and its correction for electrode resistance (eq 8). (b) Current–voltage data for varying initial ion concentrations with fitted curves based on the new model. (c) Dimensionless voltage–current curves with an inset showing the data collapse at lower voltages. The bottom row presents the scaling of the fitting parameters with salt concentration c_0 (blue points): (d) limiting current I_{lim}, (e) series resistance R_s, and (f) overlimiting conductance σ_{OLC} compared to theoretical curves (solid colors) and scalings (slopes) discussed in the text.

RESULTS

Current–Voltage Relation. A typical voltammogram is shown in Figure 5a (black curve) for c_0 = 1 M. As in all prior experiments with ion-exchange membranes[10] and microfluidic devices,[17,21,23] the classical diffusion-limited behavior of eq 1 (gray line in Figure 5), which has no free parameters and saturates at the thermal voltage k_BT/e = 26 mV, does not match the data. In our experiment, we resolve this discrepancy by accounting for the electrode and reservoir polarization. A series resistance, R_s, is fitted to the low-voltage portion of each voltammogram by replacing the applied voltage, V_{app}, with

$$V = V_{app} - IR_s \quad (8)$$

in eq 1, as in the blue curve in Figure 5a. From the experiments we are thus able to infer the electrokinetic response of the glass frit, which can be separated from all the other internal resistances by examining the scalings of I_{lim}, R_s, and σ_{OLC} with salt concentration and surface charge.

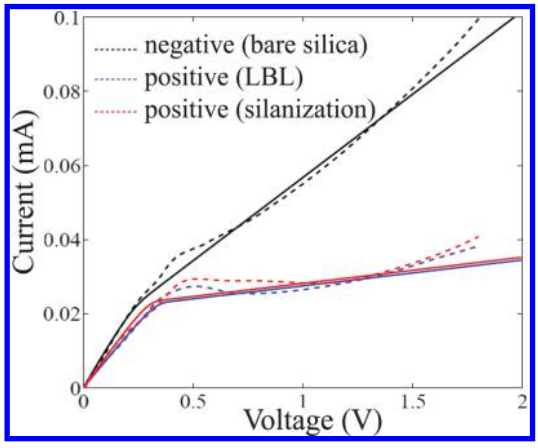

Figure 6. Effect of surface charge modification. Linear sweep voltammetry at 2 mV/s for 1 mM aqueous $CuSO_4$ solution in the same apparatus above is shown for negatively charged bare silica and two positively charged surfaces, obtained by silanization and polymer deposition. Dashed curves indicate the data, and solid lines indicate the fit to the theory (eqs 3 and 8).

After correcting for electrode polarization, the theoretical prediction of eq 3 provides a good fit of the data (red line in Figure 5a). By least-squares fitting of only three parameters (I_{lim}, R_s, and σ_{OLC}) for each quasi-steady voltammogram, the coefficient of determination is 99% over a wide range of salt concentrations (Figure 5b). The limiting current from the fitting for 1 M concentration is about 6.8 mA, and the membrane working area is the same as the cross-sectional area of the glass frit, resulting in a calculated limiting current density of approximately 8.6 mA/cm^2. As shown in Figure 5c, the dimensionless current, $\tilde{I} = I/I_{lim}$, versus voltage, $\tilde{V} = zeV/k_BT$ (z = 2), collapses onto a single master curve, eq 1, at low voltage (inset) while displaying a nearly constant overlimiting conductance, consistent with the theory.[12] For the lowest salt concentration (10^{-4} M), a nonconstant overlimiting conductance could also be related to additional ion transport from the dissociation of water or dissolved CO_2 in the solution, but transient diffusion is the more likely cause of the observed weak oscillations around the mean linear profile of OLC at all salt concentrations, as discussed above and in the Supporting Information.

Limiting Current. To the best of our knowledge, this is the first quantitative fit of experimental data by OLC theory by any mechanism. To check our assumptions and identify the physical mechanism for OLC, the scalings of I_{lim}, R_s, and σ_{OLC} are investigated with respect to the concentration of $CuSO_4$ over 4 orders of magnitude, from 0.1 mM to 1.0 M. The error in each

dx.doi.org/10.1021/la4040547 | Langmuir 2013, 29, 16167–16177

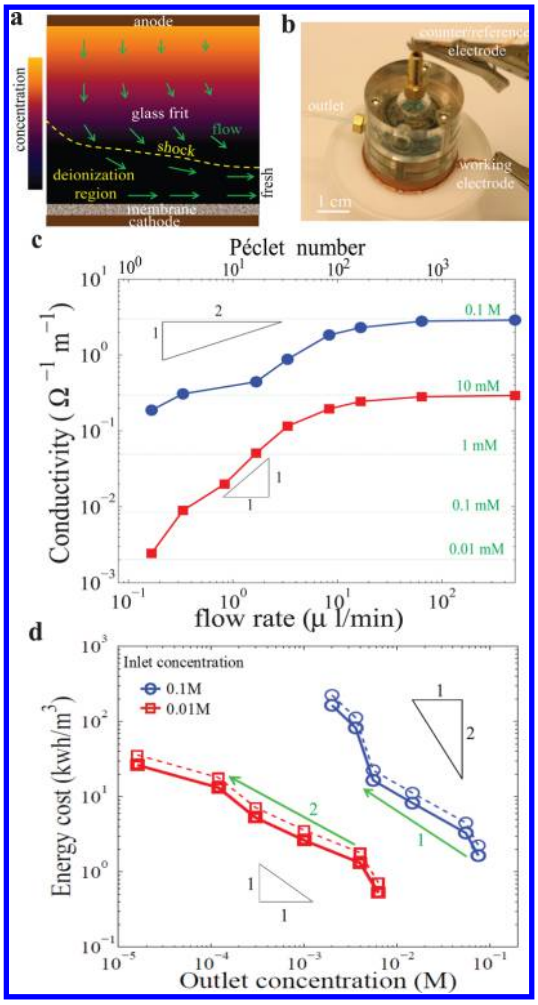

Figure 7. Water deionization by shock electrodialysis operating under OLC. (a) Schematic of the extraction flow and salt concentration profile. (b) Photograph of the button-cell device. (c) Conductivity (y axis) and salt concentration (green lines) of the extracted water versus flow rate, with theoretical scalings from eq 12. (d) Energy cost per volume with (dashed lines) and without (solid lines) the series resistance attributed to the reservoir and electrodes for the same experiments.

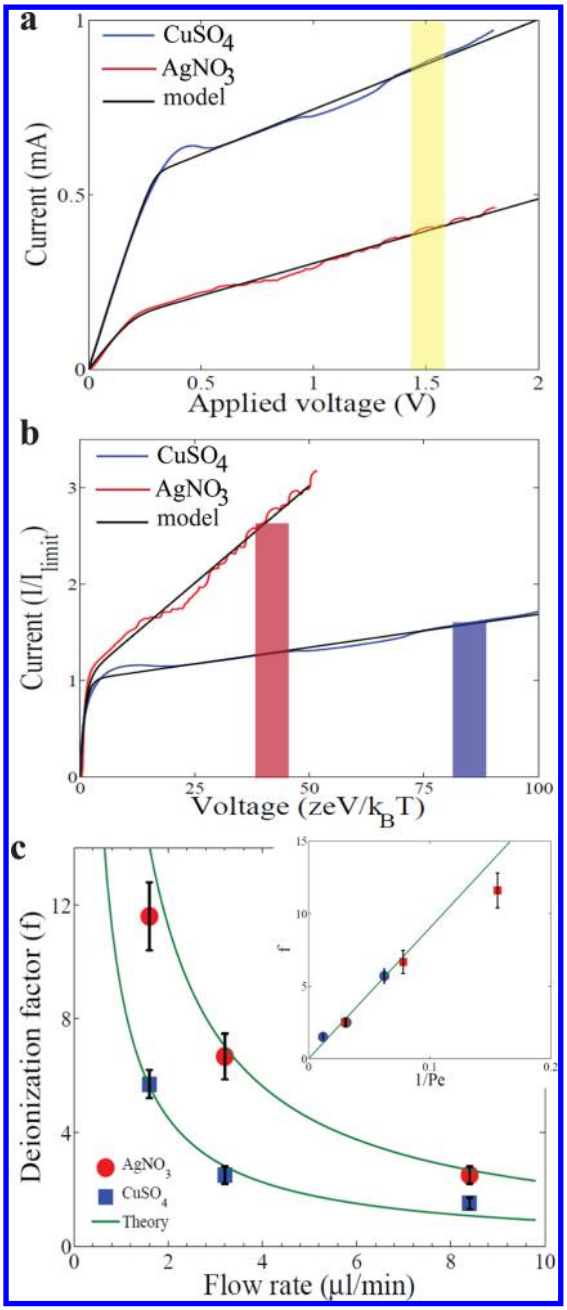

Figure 8. Overlimiting current and shock electrodialysis with 10 mM silver nitrate using the device in Figure 3. The current–voltage relation in plot a exhibits a similar constant overlimiting conductance, similar to that of 10 mM copper sulfate, but with a smaller limiting current and voltage scale, which lead to a larger dimensionless current in plot b. Bars indicate data taken at V_{app} = 1.5 V. The deionization factor in plot c is larger in $AgNO_3$ than in $CuSO_4$ at the same voltage, flow rate, and salt concentration, as predicted by the scaling theory, eq 12 (solid curves and inset data collapse).

data point (from the Supporting Information) is on the order of 10%, which is smaller than the point size in the log–log plots of Figure 5d–f showing power-law scalings.

According to dilute solution theory, eq 2, the limiting current, I_{lim}, is linearly proportional to concentration. The fitted I_{lim} (Figure 5d) verifies this scaling at low concentration and deviates to lower values at high concentration, consistent with reduced Cu^{2+} activity and diffusivity.[45] A simple estimate (red curve), using free-solution values[46] D_0 for $D(c_0)$ in eq 2, captures the scaling of the data for $I_{lim}(c_0)$ well. In the Bruggeman approximation, however, the macroscopic diffusivity $D_m = \varepsilon^{3/2}D_0$ at low concentration is ≈13 times smaller than the apparent dispersion D from eq 2. The discrepancy partially reflects transient diffusion (an effectively smaller L) because the diffusion distance $2(D_m t)^{1/2} \approx 0.5$ mm when the limiting current is reached is somewhat smaller than the frit thickness, L = 1 mm.

Consistent with our analysis of OLC below, the leading cause of the enhanced dispersion inferred from I_{lim} may be electroosmotic convection in the glass frit. Electroosmotic flow toward the impermeable membrane/cathode structure is balanced by a pressure-driven back flow that produces dispersion.[19] Taylor dispersion is negligible on the basis of the formula for a single cylindrical pore, $D_{Taylor}/D_m - 1 = \varepsilon_p^{3/2}Pe_1^2/48 \sim 0.01$, even using a large EOF velocity of U = 400 μm/s in the single-channel Péclet number $Pe_1 = Uh_p/D_0$. For a network of pores, however, there is additional dispersion due to the randomness in streamline topology[47] (also referred to as eddy diffusion or dispersion[48]). Indeed, the simple estimate

dx.doi.org/10.1021/la4040547 | Langmuir 2013, 29, 16167–16177

$D_{eddy}/D_m \approx Pe_e/2 \approx 10$ could explain the fitting result for D above where we use the same velocity and a mean loop size of $h_{loop} = 25\ \mu m$, consistent with Figure 3c in estimating the eddy Péclet number, $Pe_e = Uh_{loop}/D_m$. We have also confirmed that replacing the silica glass frit with a loopless porous medium (an anodic aluminum oxide membrane with straight pores of 200 nm diameter) leads to a reduced I_{lim} consistent with $D_m \approx D_0$, as will be reported elsewhere (Han, J.-H.; Bai, P.; Khoo, E.; Bazant, M. Z., to be submitted for publication).

Series Resistance. The series resistance R_s can be attributed to two primary sources: the Ohmic resistance of the reservoir, R_{res}, at low salt and the Faradaic resistance of the anode, R_F, at high salt. (The cathode Faradaic resistance is reduced by contact with the Nafion membrane.) Neglecting ICP and assuming equal ionic diffusivities, we estimate the reservoir resistance using

$$R_{res} = \frac{k_B T L}{2\pi R^2 (ze)^2\, D(c_0) c_0} \tag{9}$$

Assuming linearized Butler–Volmer kinetics, we estimate the anode Faradaic resistance as

$$R_F = \frac{k_B T}{n e I_0} = \frac{k_B T}{2 e K_0 {c_0}^{1/2}} \tag{10}$$

where $I_0 = K_0 c_0^{\alpha_c}$ is the exchange current density. The transfer coefficient is $\alpha_c = {}^1/_2$ for the rate-limiting transfer of 1 out of $n = 2$ electrons.[38,39] The data in Figure 5e is quantitatively consistent with the theory, $R_s = R_{res} + R_F$ (red curve), with a fitted prefactor of $K_0 = 2.8\ A/m^2$ (for molar c_0). The measured exchange current $I_0 = 3.9\ A/m^2$ at $c_0 = 0.5$ M is close to $I_0 = 9.7\ A/m^2$ from recent experiments with $CuSO_4$ at neutral pH[43] (which is below I_0 in strong acids[38,39]). We are thus able to attribute the remaining voltage V in eq 8, which exhibits OLC (eq 3), to the glass frit.

Overlimiting Current. The SC and EOF mechanisms for OLC are distinguished by different scalings in eq 6 with salt concentration c_0 and surface charge density, q_s. In the absence of flow, the overlimiting conductance from surface conduction is given by eq 4.[12] Using $D = \varepsilon_p{}^{3/2} D_m$, the theoretical line with constant q_s (green dashed line) roughly matches the experimental value at the lowest salt concentration but lies far below the data at higher concentrations (blue points) in Figure 5f. This is consistent with the prediction that SC becomes important only at low salt concentrations,[12] but we must also consider the effect of charge regulation. It is well known that that the surface charge of silica is regulated by the dissociation of silanol groups,[34,41,42]

$$SiOH \leftrightarrow SiO^- + H^+ \ (pK = 7.5) \tag{11}$$

Using the Gouy–Chapman–Stern model to obtain the surface pH,[41] we can calculate the surface charge from the measured bulk pH versus salt concentration, assuming $pK = 7.5$ for silica. (Details are in the Supporting Information, where it is also shown that the pK has little effect on the prediction of OLC.) As shown in Figure 5f (green dotted curve), the decrease in q_s with increasing c_0 leads to the opposite trend from the experimental data. We conclude that SC is not the primary mechanism for OLC in our experiments, although it may contribute at low salt concentration.

Because the data cannot be explained by SC, the theory suggests that EOF is the likely mechanism. In a parallel-plate microchannel, the transition from SC to EOF is predicted to occur at a thickness of 8 μm (for $c_0 = 1$ M, $L = 1$ mm),[12] which is comparable to the mean effective cylindrical pore diameter of the silica frit, $4h_p = 2.3\ \mu m$. As noted above, the single-channel analysis underestimates the true effect of EOF in a heterogeneous porous medium because there are eddies around loops in the pore network (Figure 2) whose size $h_e \gg h_p$ could reach tens of micrometers in our silica frit, thus making EOF dominant.

Indeed, the EOF scaling theory is consistent with the experimental data. If we fit h_e to the lowest concentration data point using the theoretical formula eq 5 with $D_m = (0.4)^{3/2} D_0$ and $D_0 = 8.5 \times 10^{-6}\ cm^2/s$[46] and all other parameters known, then we obtain an eddy size of $h_e = 100\ \mu m$, comparable to the thickness of the depleted region,[12] $(1 - I_{lim}/I)L$ for $I = 1.1 I_{lim}$, but this neglects the unknown numerical prefactor in eq 5. We expect this prefactor to be smaller than 1 in order to obtain a mean eddy size in the 5–50 μm range, consistent with the scale of loops in the glass frit (set by aggregates of sintered particles seen in the SEM images (Figure 3)). This range is also consistent with the characteristic eddy size inferred from the effects of hydrodynamic dispersion on I_{lim} above.

Remarkably, without any adjustable parameters, the EOF scaling theory (eq 5) accurately predicts the observed dependence on salt concentration, varying over 4 orders of magnitude, $c_0 = 0.1$ mM–1.0 M. With constant q_s (red dashed line in Figure 5f), the experiments reveal the nontrivial scaling, $\sigma_{OLC} \sim c_0^{4/5}$, at low salt concentration, and the predicted effect of surface charge regulation $\sigma_{OLC} \sim q_s(c_0)^{2/5}$ also captures the trend at high concentration (red solid curve in Figure 5f). We conclude that EOF is the likely mechanism for OLC in our experiments.

Surface Charge Modification. The dependence on surface charge density, q_s, was tested indirectly by varying the pH and modeling proton adsorption,[34,41,42] but two chemical modifications, silanization[49,50] and charged polymer deposition,[51,52] provide more direct evidence. (See the Supporting Information for details.) The current–voltage responses (Figure 6) are again fit to eqs 3 and 8. As expected, because I_{lim} is associated with bulk transport and R_s is associated with reservoir and electrode resistances, each is independent of q_s. Theory predicts that σ_{OLC} is largest for $q_s < 0$, and indeed we find an order-of-magntiude reduction for both surfaces with $q_s > 0$.

An unexpected finding is that the positive frits exhibit OLC, although it is much smaller than that of the negative silica frit. This should not occur in positive nanopores where SC acts to oppose the current. For larger, positive pores, however, OLC is possible because EOF eddies can still transport salt faster than diffusion, only rotating in the opposite sense and fighting against SC.

Water Deionization. To complement the electrochemical evidence, we experimentally verify the extreme salt depletion associated with OLC[12] by driving a flow that produces a deionization shock.[27] In microfluidic devices with tiny (nanoliter) volumes, salt concentration is typically inferred by the optical detection of fluorescent particles,[18,20,22,23,25] but here we can directly extract macroscopic (0.01–1.0 mL) samples of deionized water from the glass frit (Figure 7a) and test their conductivity by impedance spectroscopy. A proof-of-concept device (Figure 7b) is equipped with a circular outlet ($d = 0.5$ mm in diameter) at one point on the side of the frit just above the membrane, leading to an annular collection channel connected to the device outlet (Figure 3e). The volumetric

dx.doi.org/10.1021/la4040547 | Langmuir 2013, 29, 16167–16177

flow rate (Q) is controlled by a syringe pump. Two sets of experiments are conducted with initial concentrations of 100 and 10 mM, holding the applied voltage constant at V_{app} = 1.5 V, well into the OLC regime (Figure 3). The current remains steady for hours, indicating stable continuous operation during deionization. (See the Supporting Information on chronoamperometry.)

At low flow rates, we find that the salt concentration can be reduced by 4 orders of magnitude to 15 μM (Figure 7c). Essentially all of the $CuSO_4$ ions are removed, down to the level of the water ions (pH ≈5.5) and below the U.S. regulatory limit for copper in drinking water (<0.02 mM).[53] As in Figure 1d, the region of deionization (>0.5 mm) near the outlet extends across more than half of the frit thickness (1.0 mm) and is maintained in the outgoing flow. This establishes the existence of a stable deionization shock propagating against the flow (in the moving frame of reference)[24,25] over a macroscopic distance in the porous medium.[27] Such extreme deionization propagating so far into the frit cannot be explained by theories of ED based on convection−diffusion in neutral electrolytes.[9]

This observation suggests the possibility of harnessing deionization shocks in porous media for water purification. Although our apparatus has not been optimized for this purpose, it serves to illustrate the principles of shock electrodialysis. The basic idea is to drive over-limiting current through a porous medium and extract deionized water between the membrane and the shock with a pressure-driven cross-flow. In a scalable system for continuous operation (discussed below), additional outlets must also collect brine from the frit (deflected by the shock) and reaction products from electrode streams (such as hydrogen and oxygen from water splitting, as in standard ED). Here, we have just one, small freshwater outlet and negligible brine accumulation at the anode, but this suffices to demonstrate the general trade-off between flow rate and deionization[29] (Figure 7c): For a given geometry and current, the flow rate must be small enough to allow the shock to propagate across the outlet in order to deionize the outgoing stream fully. As the flow rate is increased, the shock retracts toward the membrane and crosses the outlet, thereby causing the salty fluid from the diffusion layer to be mixed with the deionized fluid behind the shock.

Flow-Rate Dependence. At fixed voltage, the deionization factor $f = c_0/c_{out}$ (ratio of inlet to outlet salt concentrations) is controlled by the Péclet number, $Pe = Ud/D = Q/dD$, where U is the mean outlet velocity. In our apparatus (Figure 3e), asymmetric flow leads to complicated concentration profiles (Figure 7a), but we can use similar solutions for simple uniform flows to understand the scaling of f for $Pe \gg 1$ (Figure 7c). For the SC mechanism, the shock has a self-similar nested boundary layer structure consisting of an outer convection−diffusion layer (or diffusive wave[54]) and an inner depleted region whose overall thickness (distance from the membrane) scales as $Pe^{-\gamma}$, where $\gamma = 1$ for uniform normal flow through the membrane[29] and $\gamma = {}^1/_2$ for uniform cross-flow along the membrane (Mani and Bazant, to be submitted for publication). Integrating the self-similar concentration profile over a fixed-diameter outlet then implies the scaling

$$f = \frac{c_0}{c_{out}} \sim Pe^{-\gamma} \sim \left(\frac{D}{Q}\right)^{\gamma} \tag{12}$$

with ${}^1/_2 \leq \gamma \leq 1$ for the SC mechanism with pressure-driven flow. For the EOF mechanism in a microchannel without net flow,[12] the depleted region has nearly uniform mean concentration scaling as $c_d/c_0 \sim (I/I_{lim})^{\nu}$, where $\nu \sim 0.3$ to 0.4. Although the theory needs to be extended for porous media and pressure-driven net flow, this result with $I/I_{lim} \sim Pe^{\gamma}$ (for the convection−diffusion layer) and $f \sim \tilde{c}_d^{-1}$ (if the depleted region spans the outlet) suggests that exponent γ in eq 12 may be replaced by the smaller value $\gamma\nu$ for the EOF.

Both sets of experiments show the expected trend of the deionization factor with the flow rate (Figure 7c). The conductivity of the inlet and outlet solutions is measured by impedance and calibrated against solutions of known salt concentration. (See the Supporting Information.) At the lowest flow rate, on the order of 0.1 μL/min, we obtain $f > 10$ starting from c_0 = 0.1 M and $f \approx 10^2$ starting from c_0 = 10 mM. At each flow rate, the solution with the lower initial ion concentration (10 mM) consistently yields a greater percentage reduction of conductivity (or concentration) than that of the higher initial ion concentration (100 mM). The larger deionization factor results from the larger dimensionless current (I/I_{lim}) and more extended deionization region (or shock) at lower salt concentrations, consistent with the theory.[12] This trend is also a consequence of mass balance, $f \sim I/(Qc_0)$, as in standard ED.

Energy Efficiency. The energy cost per volume of deionized water in the experiments of Figure 7c is plotted in Figure 7d versus the outlet concentration c_{out}. Comparing the energy cost with (dashed line) and without (solid line) the electrode and reservoir series resistances shows that less than half of the total energy cost is spent driving the copper reactions. As in standard ED, such electrode resistances can be made negligible compared to a larger total voltage in a scalable, multilayer system (Figure 9). As indicated by the green arrows, the button cell can desalinate brackish water (0.1 M) to produce potable water (<10 mM) at a cost of ≈10 kWh/m^3 and then deionize close to 0.01 mM in a second step at roughly the same cost. The net energy cost of ≈20 kWh/m^3 is well above the thermodynamic limit of ≈0.15 kWh/m^3, but this is mainly a consequence of the experimental geometry, which was not designed for this purpose.

To boost the efficiency in a practical shock ED system, the cross-flow must cover as much of the active area (drawing current) as possible. Because our device has a point outlet from the frit at only one azimuthal angle rather than a gap spanning its circumference, fluid is extracted from only a very small area, $\approx \pi d^2/2$, which is roughly ${}^1/_{50}$ of the total cell area πR^2. As a result, the total power use is nearly independent of the flow rate, and the energy/volume = power/(flow rate) should scale as $Pe^{1-} \approx f^{1/\gamma}$ from eq 12, which is consistent with the data in Figure 7d. With uniform cross-flow covering the entire active area as in Figure 9, the energy cost could, in principle, be reduced by the same factor to ≈1 kWh/m^3. This suggests that shock ED has the potential to be competitive with other approaches on efficiency while having some other possible advantages in separations discussed below.

Electrolyte Dependence. Until this point, our copper electrolytic cell has provided a convenient model system to establish the basic principles of shock ED, but the method is much more general and can be applied to arbitrary electrolytic solutions. As in standard ED, the electrodes can be chosen to drive any desired brine-producing reactions, such as water electrolysis, while the current is carried across a stack of many membranes by the input solution (see below). In our device, we have only one separation layer and copper electrodes, but we

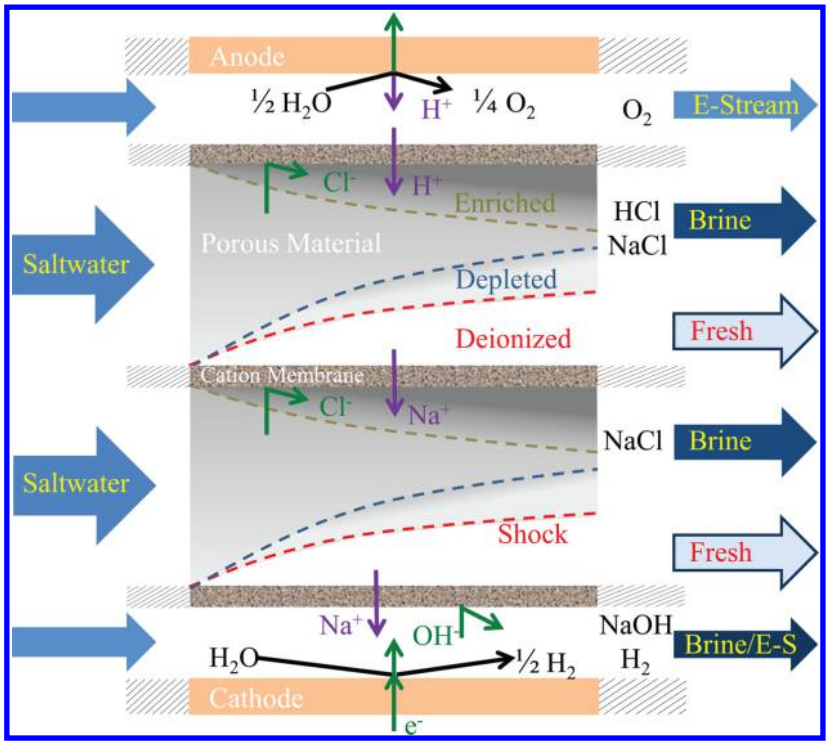

Figure 9. Sketch of a scalable shock electrodialysis system, motivated by our experimental results.

can consider a different electrodeposition reaction. In the same device, we remove silver ions from 10 mM silver nitrate ($AgNO_3$) through a porous frit and a Nafion membrane by silver deposition at the cathode. The current is sustained by copper dissolution at the anode without allowing sufficient time for ICP to cross the reservoir and reach the frit during a voltage sweep.

The results in Figure 8 are similar for both electrolytes and consistent with the theory, thereby showing the generality of the phenomenon. The raw current–voltage data (Figure 8a) indicates a slightly smaller overlimiting conductance and a much smaller limiting current for $AgNO_3$, as suggested by the scaling $I_{lim} \sim zD$. ($D_{AgNO_3} = 1.68 \times 10^{-5}$ cm^2/s[55] and $D_{CuSO_4} = 6.75 \times 10^{-6}$ cm^2/s[46] at 10 mM.) At the same voltage, $V_{app} = 1.5$ V (bars in Figure 8b), the dimensionless voltage $\tilde{V}$ is also smaller by a factor of 2 (for monovalent vs divalent cations), and the dimensionless current $\tilde{I} = 2.6$ for $AgNO_3$ is larger than $\tilde{I} = 1.6$ for $CuSO_4$, which implies a wider depletion zone, scaling as $(1 - \tilde{I}^{-1})$. During water extraction, the dependencies of the deionization factor on flow rate and diffusivity are nicely captured by the simple scaling of eq 12, as shown in Figure 8c.

DISCUSSION

Our primary finding is that thin double layers in porous media can enable faster ionic transport, leading to new surface-driven mechanisms for OLC based on SC and EOF. In particular, electroconvection driven by EOF can sustain OLC in a heterogeneous porous medium with micrometer-scale pores pressed against an impermeable electrodialysis membrane. The onset of OLC is associated with a macroscopic region of deionization within the pores (outside the double layers), which can propagate against pressure-driven flow like a shock wave. In steady state, the overlimiting conductance is approximately constant (aside from surface charge regulation), in spite of enormous spatial variations in conductivity (up to 3 orders of magnitude). These surprising phenomena are in stark contrast to the constant conductivity of ion-exchange membranes with smaller pores and overlapping (thick) double layers.

The nonlinear electrokinetic properties of porous media can be exploited for separations. Our proof-of-concept experiments (Figures 7 and 8) show that deionized water can be continuously extracted from salty water via a porous medium sustaining OLC. It is beyond the scope of this article to build and test a practical desalination system with electrode streams, but a possible design for a scalable shock ED system is shown in Figure 9. A stack of two (or more) separation layers of negatively charged porous media separated by cation exchange membranes sustains an overlimiting current. In each layer, the input solution (e.g., NaCl) undergoes salt enrichment near one membrane and salt depletion with a deionization shock near the other. In pressure-driven cross-flow, these regions are continuously separated into fresh and brine streams upon leaving the porous medium. By varying the position of the fresh/brine stream splitting in each porous layer, high water recovery (wide shock) can be traded against low energy cost (thin shock). As in standard ED, direct current can be sustained at the electrodes by water splitting (or other) reactions whose overpotential becomes negligible compared to the total voltage as the stack size increases.

Besides water deionization, such a system may also find applications in brine concentration (e.g., for salt precipitation or forward osmosis) or in nanoparticle separations. Because the separation occurs within the porous medium in cross-flow, the membrane removing ions is electrokinetically shielded and may resist fouling (which is a concern for other desalination methods[1,4]). Membraneless designs with layered porous media of different pore sizes (analogous to micro/nanochannel junctions[20,23,25]) may also be possible. Clogging by incoming particles or brine precipitates could be managed by reverse bias,

dx.doi.org/10.1021/la4040547 | Langmuir 2013, 29, 16167–16177

cleaning, or replacement due to the low cost of the porous materials themselves.

By combining microfiltration and deionization in one step, shock ED may also enable more compact, portable point-of-use systems. Besides filtration by size, suspended particles are also strongly filtered by charge. Co-ionic particles (with the same charge as the pore walls and the membrane) are repelled by the shock,[22] but counterionic particles are accelerated through the depleted region by the large electric field and sent to the outlet if they are blocked by the membrane. Some of these advantages are also possessed by microfluidic desalination devices with aligned flow and current in individual microchannels[23] but with higher fabrication costs and smaller flow rates (even with massive parallelization). By decoupling the flow and current directions using porous media, it is possible to extend deionization and filtering cheaply over macroscopic volumes.

Selective ion exchange and separation may also be possible by shock ED. In contrast to existing methods for heavy metal removal based on adsorption in nanocrystals,[8] functionalized porous media,[56,57] and biosorbents,[6,7] shock ED is not limited to particular ions and exhibits ion selectivity (based on surface transport in porous media), which could be used to fractionate different metal ions and/or charged macromolecules by splitting streams in cross-flow through the cell. Multivalent/monovalent ion separation can also be achieved by electro-osmotic convection in nanochannels[58] or by the capacitive charging of porous electrodes,[59] but shock ED could enable continuous, scalable separations based on both size and charge.

■ ASSOCIATED CONTENT

Supporting Information

Sweep rate effect for linear sweep voltammetry. Reproducibility of the measured current−voltage curves. Comparison of current−voltage curves with and without a glass frit. Chronoamperometry measurement during the deionization extraction. Impedance measurement for solution conductivity. Measurement of pH , calculation of surface charge density, and pK effect. Surface chemical modifications. This material is available free of charge via the Internet at http://pubs.acs.org.

■ AUTHOR INFORMATION

Corresponding Author

*E-mail: bazant@mit.edu.

Present Addresses

[§]Department of Surgery, Beth Israel Deaconess Medical Center, Harvard Medical School, Boston, Massachusetts 02215, United States, and Wyss Institute of Biologically Inspired Engineering, Harvard University, Boston, Massachusetts 02215, United States.

[∥]Department of Mechanical Engineering, Stanford University, Stanford, California 94304, United States.

[⊥]Blaustein Institutes for Desert Research, Ben-Gurion University of the Negev, Sede Boqer Campus, 84990 Israel.

Notes

The authors declare no competing financial interest.

■ ACKNOWLEDGMENTS

This work was supported by a grant from Weatherford International through the MIT Energy Initiative. B.Z. and M.Z.B. also acknowledge support from the USA-Israel Binational Science Foundation (grant 2010199) and J.-H.H. acknowledges support from the Basic Science Research Program through the National Research Foundation of Korea (NRF) funded by the Ministry of Education (2012R1A6A3A03039224). We thank P. Morley and A. Gallant at the MIT Central Machine Shop for producing the prototype.

■ REFERENCES

(1) Shannon, M. A.; Bohn, P. W.; Elimelech, M.; Georgiadis, J. G.; Marioas, B. J.; Mayes, A. M. Science and technology for water purification in the coming decades. *Nature* **2008**, *452*, 301−310.

(2) Humplik, T.; Lee, J.; O'Hern, S. C.; Fellman, B. A.; Baig, M. A.; Hassan, S. F.; Atieh, M. A.; Rahman, F.; Laoui, T.; Karnik, R.; Wang, E. N. Nanostructured materials for water desalination. *Nanotechnology* **2011**, *22*, 292001.

(3) Greenlee, L. F.; Lawler, D. F.; Freeman, B. D.; Marrot, B.; Moulin, P. Reverse osmosis desalination: water sources, technology, and today's challenges. *Water Res.* **2009**, *43*, 2317−2348.

(4) Potts, D. E.; Ahlert, R. C.; Wang, S. S. A critical review of fouling of reverse osmosis membranes. *Desalination* **1981**, *36*, 235−264.

(5) Schultz, A. *Hydraulic Fracturing and Natural Gas Drilling: Questions and Concerns*; Nova Science Publishers: New York, 2011.

(6) Volesky, B.; Holant, Z. R. Biosorption of heavy metals. *Biotechnol. Prog.* **1995**, *11*, 235−250.

(7) Wan Ngah, W. S.; Hanafiah, M. A. Removal of heavy metal ions from wastewater by chemically modified plant wastes as adsorbents: a review. *Bioresour. Technol.* **2008**, *99*, 3935−3948.

(8) Yavuz, C. T.; Mayo, J. T.; Yu, W. W.; Prakash, A.; Falkner, J. C.; Yean, S.; Cong, L.; Shipley, H. J.; Kan, A.; Tomson, M.; Natelson, D.; Colvin, V. L. Low-field magnetic separation of monodisperse Fe_3O_4 nanocrystals. *Science* **2006**, *314*, 964−967.

(9) Probstein, R. *Physicochemical Hydrodynamics*, 2nd ed.; John Wiley & Sons: New York, 1994.

(10) Nikonenko, V.; Pismenskaya, N.; Belova, E.; Sistat, P.; Huguet, P.; Pourcelly, G.; Larchet, C. Intensive current transfer in membrane systems: Modeling, mechanisms and application in electrodialysis. *Adv. Colloid Interface Sci.* **2010**, *160*, 101−123.

(11) Porada, S.; Zhao, R.; van der Wal, A.; Presser, V.; Biesheuvel, P. Review on the science and technology of water desalination by capacitive deionization. *Prog. Mater. Sci.* **2013**, *58*, 1388−1442.

(12) Dydek, E. V.; Zaltzman, B.; Rubinstein, I.; Deng, D. S.; Mani, A.; Bazant, M. Z. Overlimiting current in a microchannel. *Phys. Rev. Lett.* **2011**, *107*, 118301.

(13) Rubinstein, I.; Warshawsky, A.; Schechtman, L.; Kedem, O. Elimination of acid-base generation (water-splitting) in electrodialysis. *Desalination* **1984**, *51*, 55−60.

(14) Andersen, M. B.; van Soestbergen, M.; Mani, A.; Bruus, H.; Biesheuvel, P. M.; Bazant, M. Z. Current induced membrane discharge. *Phys. Rev. Lett.* **2012**, *109*, 108301.

(15) Rubinstein, I.; Staude, E.; Kedem, O. Role of the membrane surface in concentration polarization at ion-exchange membrane. *Desalination* **1988**, *69*, 101−114.

(16) Zaltzman, B.; Rubinstein, I. Electro-osmotic slip and electro-convective instability. *J. Fluid Mech.* **2007**, *579*, 173−226.

(17) Rubinstein, S.; Manukyan, G.; Staicu, A.; Rubinstein, I.; Zaltzman, B.; Lammertink, R.; Mugele, F.; Wessling, M. Direct observation of a nonequilibrium electro-osmotic instability. *Phys. Rev. Lett.* **2008**, *101*, 236101.

(18) Yossifon, G.; Chang, H.-C. Selection of non-equilibrium overlimiting currents: universal depletion layer formation dynamics and vortex instability. *Phys. Rev. Lett.* **2008**, *101*, 254501.

(19) Yaroshchuk, A.; Zholkovskiy, E.; Pogodin, S.; Baulin, V. Coupled concentration polarization and electroosmotic circulation near micro/nanointerfaces: Taylor-Aris model of hydrodynamic dispersion and limits of its applicability. *Langmuir* **2011**, *27*, 11710−11721.

(20) Kim, S. J.; Wang, Y.; Lee, J. H.; Jang, H.; Han, J. Concentration polarization and nonlinear electrokinetic flow near a nanofluidic channel. *Phys. Rev. Lett.* **2007**, *99*, 044501.

(21) Yossifon, G.; Mushenheim, P.; Chang, H.-C. Controlling nanoslot overlimiting current with the depth of a connecting microchamber. *Europhys. Lett.* **2010**, *90*, 64004.
(22) Wang, Y.-C.; Stevens, A. L.; Han, J. Million-fold preconcentration of proteins and peptides by nanofluidic filter. *Anal. Chem.* **2005**, *77*, 4293−4299.
(23) Kim, S. J.; Ko, S. H.; Kang, K. H.; Han, J. Direct seawater desalination by ion concentration polarization. *Nat. Nanotechnol.* **2010**, *5*, 297−301.
(24) Mani, A.; Zangle, T. A.; Santiago, J. G. On the propagation of concentration polarization from microchannel/nanochannel interfaces part I: analytical model and characteristic analysis. *Langmuir* **2009**, *25*, 3898−3908.
(25) Zangle, T. A.; Mani, A.; Santiago, J. G. On the propagation of concentration polarization from microchannel/nanochannel interfaces part II: numerical and experimental study. *Langmuir* **2009**, *25*, 3909−3916.
(26) Zangle, T. A.; Mani, A.; Santiago, J. G. Theory and experiments of concentration polarization and ion focusing at microchannel and nanochannel interfaces. *Chem. Soc. Rev.* **2010**, *39*, 1014−1035.
(27) Mani, A.; Bazant, M. Z. Deionization shocks in microstructures. *Phys. Rev. E* **2011**, *84*, 061504.
(28) Yaroshchuk, A. Over-limiting currents and deionization "shocks" in current-induced polarization: local-equilibrium analysis. *Adv. Colloid Interface Sci.* **2012**, *183*−*184*, 68Ð81.
(29) Dydek, E. V.; Bazant, M. Z. Nonlinear dynamics of ion concentration polarization in porous media: The leaky membrane model. *AIChE J.* **2013**, *59*, 3539−3555.
(30) Bazant, M. Z.; Squires, T. M. Induced-charge electrokinetic phenomena. *Curr. Opin. Colloid Interface Sci.* **2010**, *15*, 203−213.
(31) Yaroshchuk, A. E. Transport properties of long straight nanochannels in electrolyte solutions: a systematic approach. *Adv. Colloid Interface Sci.* **2011**, *168*, 278−291.
(32) Yaroshchuk, A. What makes a nano-channel? A limiting-current criterion. *Microfluid. Nanofluid.* **2012**, *12*, 615−624.
(33) Rubinstein, I.; Zaltzman, B. Convective diffusive mixing in concentration polarization: from Taylor dispersion to surface convection. *J. Fluid Mech.* **2013**, *728*, 239−278.
(34) van der Heyden, F. H.; Stein, D.; Dekker, C. Streaming currents in a single nanofluidic channel. *Phys. Rev. Lett.* **2005**, *95*, 116104.
(35) Delgado, A.; González-Caballero, F.; Hunter, R.; Koopal, L.; Lyklema, J. Measurement and interpretation of electrokinetic phenomena. *J. Colloid Interface Sci.* **2007**, *309*, 194−224.
(36) Druzgalski, C. L.; Andersen, M. B.; Mani, A. Direct numerical simulation of electroconvective instability and hydrodynamic chaos near an ion-selective surface. *Phys. Fluids* **2013**, *25*, 110804.
(37) Deen, W. M. *Analysis of Transport Phenomena*, 2nd ed.; Oxford University Press: New York, 2012.
(38) Mattsson, E.; Bockris, J. O. Galvanostatic students of the kinetics of deposition and dissolution in the copper + copper sulfate system. *Trans. Faraday Soc.* **1959**, *55*, 1586−1601.
(39) Brown, O. R.; Thirsk, H. R. The rate-determining step in the electrodeposition of copper on copper from aqueous cupric sulfate solutions. *Electrochim. Acta* **1965**, *10*, 383−393.
(40) Rosso, M. Electrodeposition from a binary electrolyte: new developments and applications. *Electrochim. Acta* **2007**, *53*, 250−256.
(41) Behrens, S. H.; Grier, D. G. The charge of glass and silica surfaces. *J. Chem. Phys.* **2001**, *115*, 6716−6721.
(42) Gentil, C.; Côte, D.; Bockelmann, U. Transistor based study of the electrolyte/SiO_2 interface. *Phys. Status Solidi A* **2006**, *203*, 3412−3416.
(43) Semichaevsky, A. V.; Johnson, H. T.; Low, K.; Paul, D.; Chandra, A.; Bastawros, A. Focused electric field-induceed ion transport: experiments and modeling. *Electrochem. Solid State Lett.* **2010**, *13*, D100−D103.
(44) Huth, J. M.; Swinney, H. L.; McCormick, W. D.; Kuhn, A.; Argoul, F. Role of convection in thin-layer electrodeposition. *Phys. Rev. E* **1995**, *51*, 3444−3461.
(45) Quickenden, T. I.; Xu, Q. Z. Toward a reliable value for the diffusion coefficient of cupric ion in aqueous solution. *J. Electrochem. Soc.* **1996**, *143*, 1248−1253.
(46) Noulty, R. A.; Leaist, D. G. Diffusion in aqueous copper sulfate and copper sulfate-sulfuric acid solutions. *J. Solution Chem.* **1987**, *16*, 813−825.
(47) Koch, D. L.; Brady, J. F. Dispersion in fixed beds. *J. Fluid Mech.* **1985**, *154*, 399−427.
(48) van Deemter, J. J.; Zuiderweg, F. J.; Klinkeneerg, A. Longitudinal diffusion and resistance to mass transfer as causes of nonideality in chromatography. *Chem. Eng. Sci.* **1956**, *5*, 271−289.
(49) Jani, A. M.; Anglin, E. J.; McInnes, S. J. P.; Losic, D.; Shapter, J. G.; Voelcker, N. H. Nanoporous anodic aluminium oxide membranes with layered surface chemistry. *Chem. Commun.* **2009**, 3062−3064.
(50) Jani, A. M.; Kempson, I. M.; Losic, D.; Voelcker, N. H. Dressing in layers: layering surface functionalities in nanoporous aluminum oxide membranes. *Angew. Chem., Int. Ed.* **2010**, *49*, 7933−7937.
(51) Ai, S.; Lu, G.; He, Q.; Li, J. Highly flexible polyelectrolyte nanotubes. *J. Am. Chem. Soc.* **2003**, *125*, 11140−11141.
(52) Yeo, S. J.; Kang, H.; Kim, Y. H.; Han, S.; Yoo, P. J. Layer-by-layer assembly of polyelectrolyte multilayers in three-dimensional inverse opal structured templates. *ACS Appl. Mater. Interfaces* **2012**, *4*, 2107−2115.
(53) U.S. Environmental Protection Agency Lead and Copper Rule, Code of Federal Regulations 40 CFR Part 141, 2007.
(54) Bazant, M. Z. Regulation of ramified electrochemical growth by a diffusive wave. *Phys. Rev. E* **1995**, *52*, 1903−1914.
(55) Albright, J. G.; Miller, D. G. Mutual-diffusion coefficients at 25° in the system silver nitrate-water. *J. Phys. Chem.* **1972**, *76*, 1853−1857.
(56) Davis, M. E. Ordered porous materials for emerging applications. *Nature* **2002**, *417*, 813−821.
(57) Feng, X.; Fryxell, G. E.; Wang, L.-Q.; Kim, A. Y.; Liu, J.; Kemner, K. M. Functionalized monolayers on ordered mesoporous supports. *Science* **1997**, *276*, 923−926.
(58) Pennathur, S.; Santiago, J. G. Electrokinetic transport in nanochannels. 1. Theory. *Anal. Chem.* **2005**, *77*, 6772−6781.
(59) Zhao, R.; van Soestbergen, M.; Rijnaarts, H.; van der Wal, A.; Bazant, M.; Biesheuvel, P. Time-dependent ion selectivity in capacitive charging of porous electrodes. *J. Colloid Interface Sci.* **2012**, *384*, 38−44.